

## Contents

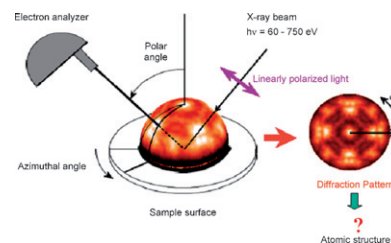
### Articles

**P.A.P. Nascente, M.F. Carazzolle, A. de Siervo, S.S. Maluf, R. Landers, G.G. Kleiman**

*Journal of Molecular Catalysis A: Chemical 281 (2008) 3*

Crystallographic structure of ultra-thin films of Pd on Ni(1 1 1) and Ni on Pd(1 1 1) studied by photoelectron diffraction

Ultra-thin films of Pd and Ni were deposited on the Ni(1 1 1) and Pd(1 1 1) surfaces, respectively, and then were characterized by X-ray photoelectron spectroscopy (XPS), low-energy electron diffraction (LEED), and X-ray photoelectron diffraction (XPD). Both Pd and Ni films grow in a layer-by-layer mode over the Ni(1 1 1) and Pd(1 1 1) surfaces at room temperature. After annealing (at 600 °C for the Pd film and 300 °C for the Ni film), adsorbate islands cover the majority of the surface and random surface alloys form the remaining surface.



**M.F. Carazzolle, G.G. Kleiman, R. Landers, A. Pancotti, A. de Siervo, E.A. Soares**

*Journal of Molecular Catalysis A: Chemical 281 (2008) 9*

Electronic structure and atomic positions of metallic surface alloys

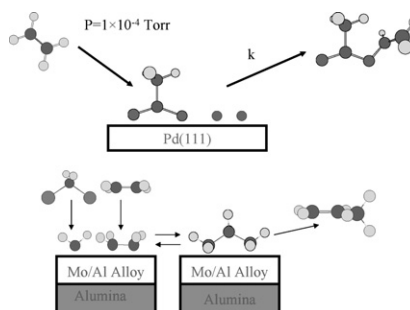
We present electronic and crystallographic structure determinations of metallic surface alloys. Core level photoemission and Auger energy shifts, which are appropriate for bulk alloys can no longer be used for surface alloys. In this case, it is possible to use the spectral form of the XPS spectra to understand the surface electron structure and XPD to determine atomic positions.

Photoelectron Spectra ⇒ Asymmetries + Satellites ⇒ Pd Local Electronic Structure  
 ↓  
 XPD ⇒ Diffraction Patterns ⇒ Atomic Positions

**Feng Gao, Yilin Wang, Florencia Calaza, Dario Stacchiola, Wilfred T. Tysoe**

*Journal of Molecular Catalysis A: Chemical 281 (2008) 14*

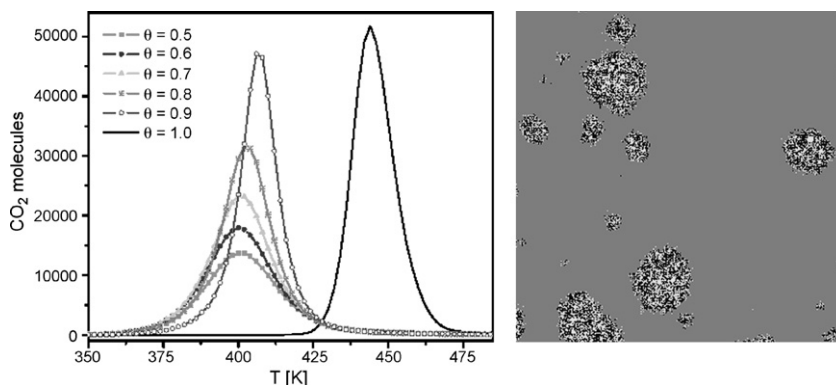
Probing reaction pathways on model catalyst surfaces: Vinyl acetate synthesis and olefin metathesis



S.J. Alas, L. Vicente

*Journal of Molecular Catalysis A: Chemical* 281 (2008) 24

Study of the “explosive” NO + CO reaction on a Pt(1 0 0) surface by dynamic Monte Carlo simulation

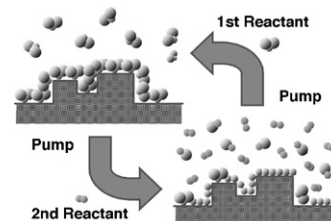


Hugo Tiznado, Menno Bouman, Byung-Chang Kang, Ilkeun Lee, Francisco Zaera

*Journal of Molecular Catalysis A: Chemical* 281 (2008) 35

Mechanistic details of atomic layer deposition (ALD) processes for metal nitride film growth

The mechanism of the surface reactions involved in the atomic layer deposition (ALD) of metal nitride films has been characterized with the aid of X-ray photoelectron and infrared spectroscopies. Metal reduction appears to occur at least in part via disproportionation of the metal precursor. That leads to the growth of non-stoichiometric films.

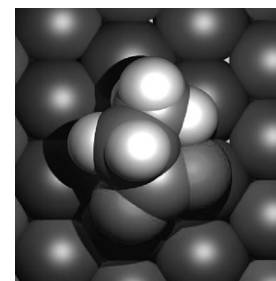


Joanna N. James, David S. Sholl

*Journal of Molecular Catalysis A: Chemical* 281 (2008) 44

Density Functional Theory studies of dehydrogenated and zwitterionic glycine and alanine on Pd and Cu surfaces

Chiral modification of achiral metal catalysts with chiral auxiliary molecules is a promising method of creating chiral surfaces for heterogeneous catalysis. The ability of a chiral template overlayer to affect the adsorption enantioselectivity of a probe molecule depends on the local adsorption geometry of the template molecule. One potential class of chiral modifier are the amino acids. Previous experimental studies demonstrated that glycine is adsorbed on the Cu(1 0 0) and Cu(1 1 0) surfaces in its dehydrogenated form,  $\text{NH}_2\text{CH}_2\text{COO}$ , at room temperature. In contrast, recent X-ray photoelectron spectroscopy experiments indicate zwitterionic adsorption of glycine to Pd(1 1 1). Using Density Functional Theory, we have studied the adsorption of glycine on Pd(1 1 1), Cu(1 0 0) and Cu(1 1 0) to examine this apparent difference in chemical states on these surfaces.

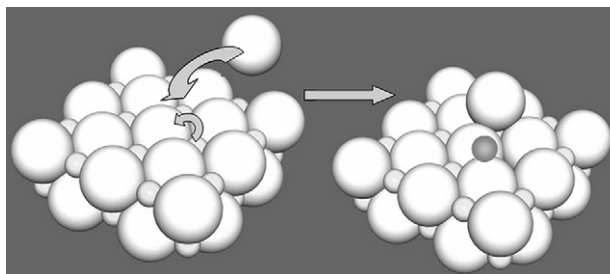


Sarah C. Petitto, Erin M. Marsh, Gregory A. Carson, Marjorie A. Langell

*Journal of Molecular Catalysis A: Chemical* 281 (2008) 49

Cobalt oxide surface chemistry: The interaction of CoO(1 0 0),  $\text{Co}_3\text{O}_4(1 1 0)$  and  $\text{Co}_3\text{O}_4(1 1 1)$  with oxygen and water

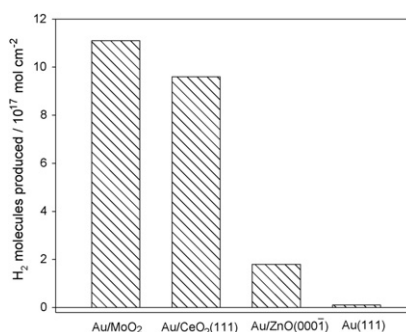
Cobalt oxides comprise two readily accessible cation oxidation states:  $\text{Co}^{2+}$  and  $\text{Co}^{3+}$  that are thermodynamically competitive under common ambient conditions.  $\text{CoO}(1 0 0)$ ,  $\text{Co}_3\text{O}_4(1 1 0)$ , and  $\text{Co}_3\text{O}_4(1 1 1)$  substrates were studied using surface sensitive techniques to determine their surface structure and reactivity towards  $\text{O}_2$  and  $\text{H}_2\text{O}$  and their stability under reducing UHV conditions.



**J.A. Rodríguez, P. Liu, J. Hrbek, M. Pérez,  
J. Evans**

*Journal of Molecular Catalysis A: Chemical* 281  
(2008) 59

Water-gas shift activity of Au and Cu nanoparticles  
supported on molybdenum oxides

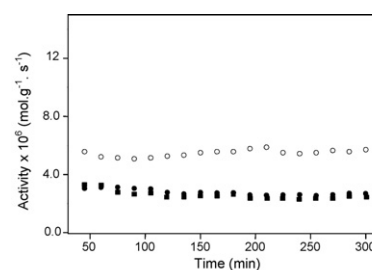


**Amalia Luz C. Pereira, Guillermo José P. Berrocal,  
Sérgio G. Marchetti, Alberto Albornoz,  
Alexilda O. de Souza, Maria do Carmo Rangel**

*Journal of Molecular Catalysis A: Chemical* 281  
(2008) 66

A comparison between the precipitation and  
impregnation methods for water gas shift catalysts

Chromium-doped magnetite was prepared by precipitation and impregnation methods, to obtain catalysts for water gas shift reaction. Chromium preserved the specific surface area during the reaction and delayed the metallic iron production but decreased the activity per area, due to its ability in making the production of Fe<sup>2+</sup> species more difficult. The impregnation method produced the most active catalyst.

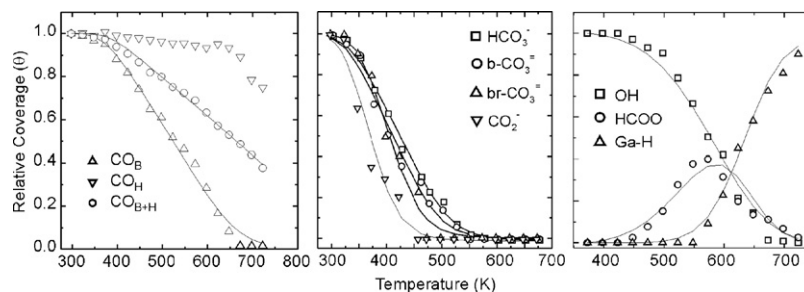


Activity of the catalysts as a function of time. • MCP sample; ○ MCI sample; ■ MP sample. M = magnetite; C = chromium; P = precipitation and I = impregnation.

**Sebastián E. Collins, Miguel A. Baltanás,  
Adrian L. Bonivardi**

*Journal of Molecular Catalysis A: Chemical* 281  
(2008) 73

Heats of adsorption and activation energies of  
surface processes measured by infrared spectroscopy

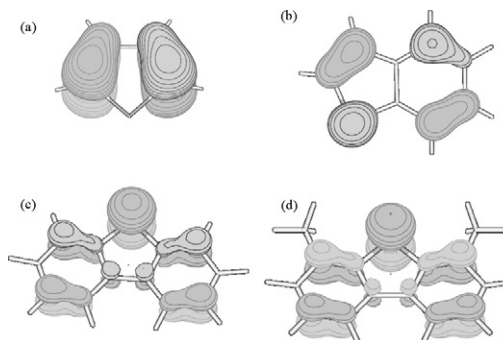


**Isidoro García-Cruz, Diego Valencia,  
Tatiana Klimova, Raúl Oviedo-Roa,  
José Manuel Martínez-Magadán,  
Rodolfo Gómez-Balderas, Francesc Illas**

*Journal of Molecular Catalysis A: Chemical* 281  
(2008) 79

Proton affinity of S-containing aromatic compounds:  
Implications for crude oil hydrosulfurization

Highest occupied molecular orbital (HOMO), (a) thiophene, (b) benzothiophene, (c) dibenzothiophene and (d) 4,6-dimethyldibenzothiophene at B3LYP/6-311++G\*\* level of theory.

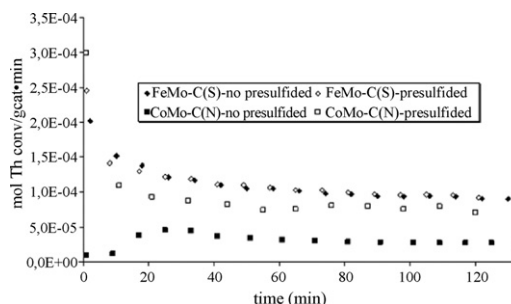


**Esneyder Puello-Polo, Joaquín L. Brito**

*Journal of Molecular Catalysis A: Chemical* 281 (2008) 85

Effect of the type of precursor and the synthesis method on thiophene hydrodesulfurization activity of activated carbon supported Fe-Mo, Co-Mo and Ni-Mo carbides

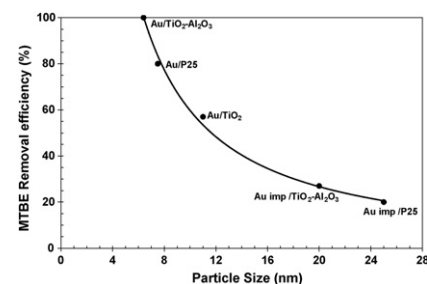
Activated carbon supported bimetallic M-Mo carbides (M = Fe, Co, Ni) derived from sulfate precursors showed high HDS activity even without sulfiding pretreatment. Similar catalysts prepared from nitrates required presulfiding in order to attain good activity levels.

**Vicente Rodríguez-González, Rodolfo Zanella, Gloria del Angel, Ricardo Gómez**

*Journal of Molecular Catalysis A: Chemical* 281 (2008) 93

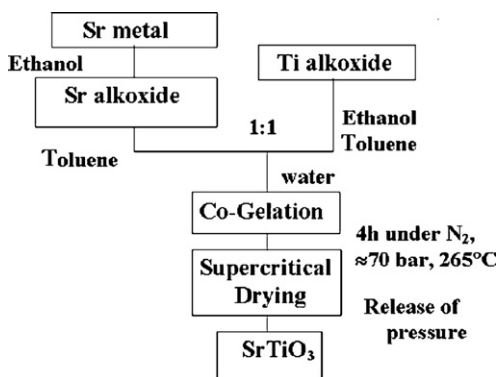
MTBE visible-light photocatalytic decomposition over Au/TiO<sub>2</sub> and Au/TiO<sub>2</sub>-Al<sub>2</sub>O<sub>3</sub> sol-gel prepared catalysts

It is shown that on supported gold photocatalysts with varying gold particle size the MTBE photodegradation expressed as TOC (total organic carbon) strongly depend on the gold particle size. The photoactivity decreases as the particle size increases. Smaller gold particles <7.0 nm are the most active for this reaction under visible-light source.

**Chih-Ang Chang, Brian Ray, Dilip K. Paul, Dmytro Demydov, Kenneth J. Klabunde**

*Journal of Molecular Catalysis A: Chemical* 281 (2008) 99

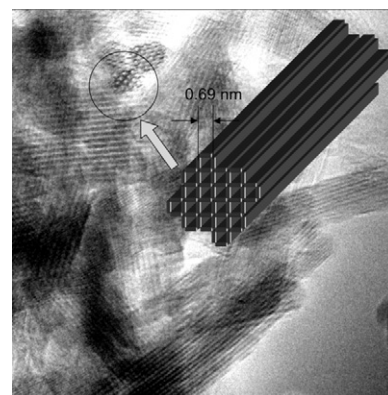
Photocatalytic reaction of acetaldehyde over SrTiO<sub>3</sub> nanoparticles

**M. Alvarez Lemus, T. López, S. Recillas, D.M. Frías, M. Montes, J.J. Delgado, M.A. Centeno, J.A. Odriozola**

*Journal of Molecular Catalysis A: Chemical* 281 (2008) 107

Photocatalytic degradation of 2,4-dichlorophenoxyacetic acid using nanocrystalline cryptomelane composite catalysts

2,4-Dichlorophenoxyacetic acid is a common systemic herbicide used in the control of broadleaf weeds. It is the third-most widely used herbicide in the world. 2,4-D heterogeneous photocatalysis has emerged as a useful process to aid remediation of wastewater contamination. Manganese oxide with 2 × 2 tunnel structure, cryptomelane show good results in the photodegradation of 2,4-D and excellent performance in the photodegradation of methylene blue. The later as a consequence of the S-Mn interaction that favours the adsorption step in the photodegradation process. The existence of microporous manganese oxide minerals with the OMS structure may be an acceptable environmental solution for the remediation of wastewaters.

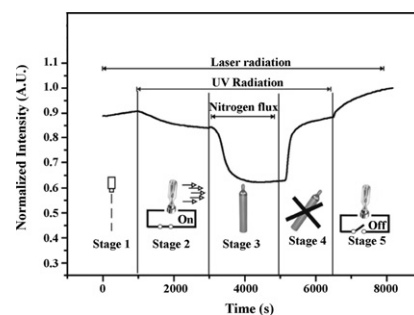


**R. Trejo-Tzab, J.J. Alvarado-Gil, P. Quintana, T. López**

*Journal of Molecular Catalysis A: Chemical* 281 (2008) 113

Study of the photoactivation of titania Degussa P25 in ethanol–methanol suspensions using a piezoelectric sensor

Photoactivation of TiO<sub>2</sub> Degussa P25 in ethanol–methanol suspensions was monitored in situ using a piezoelectric sensor. The process was studied in a specially designed cell in which the sample (in N<sub>2</sub> flux) was illuminated by a continuous UV Hg lamp to induce photoactivation. It was found that the amplitude, the initial time and the velocity of activation signal are related to ethanol–methanol mixture ratio. The associated mechanisms are discussed.

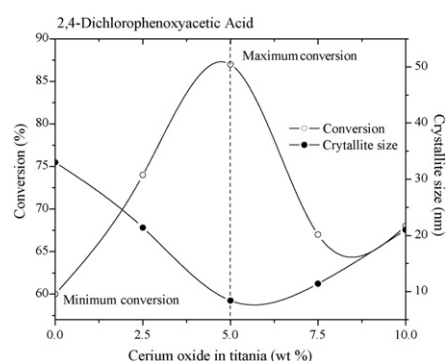


**Félix Galindo, Ricardo Gómez, Manuel Aguilar**

*Journal of Molecular Catalysis A: Chemical* 281 (2008) 119

Photodegradation of the herbicide 2,4-dichlorophenoxyacetic acid on nanocrystalline TiO<sub>2</sub>–CeO<sub>2</sub> sol–gel catalysts

Anatase crystallite size calculated from Rietveld refinement data was plotted as function of the cerium content and compared with the photocatalytic activity in the 2,4-dichlorophenoxyacetic acid decomposition. The maximum in activity corresponds to the catalyst with the smallest crystallite size.

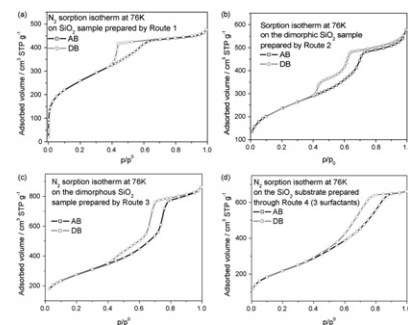


**C. Velásquez, M.L. Ojeda, A. Campero, J.M. Esparza, F. Rojas**

*Journal of Molecular Catalysis A: Chemical* 281 (2008) 126

Development and vapor sorption assessment of dimorphic SiO<sub>2</sub> porous substrates

Overall view of the N<sub>2</sub> sorption isotherms at 76 K on SiO<sub>2</sub> dimorphic and monomorphic substrates arising from the mixing of sol–gel dispersions of P123, F127, and CTAB surfactants.

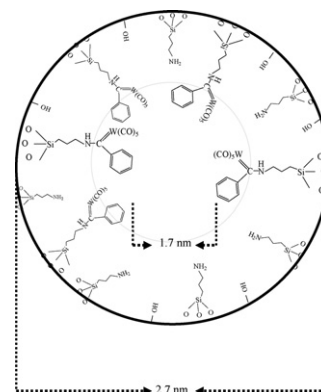


**María Luisa Ojeda, Antonio Campero, José Guadalupe López-Cortés, María Carmen Ortega-Alfaro, Celso Velásquez, Cecilio Alvarez**

*Journal of Molecular Catalysis A: Chemical* 281 (2008) 137

Covalent binding of a Fischer-type metal carbene in ordered mesoporous MCM-41-functionalized silica

Model for a tungsten Fischer carbene covalently bound to mesoporous MCM-41.





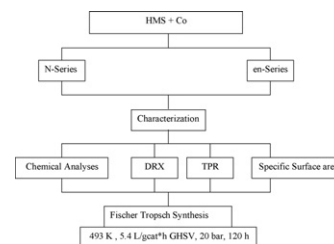
**Estephanía Lira, Carmen M. López, Freddy Oropeza, Mónica Bartolini, Juan Alvarez, Mireya Goldwasser, Francisco López Linares, Jean-François Lamonier, M. Josefina Pérez Zurita**

*Journal of Molecular Catalysis A: Chemical* 281 (2008) 146

HMS mesoporous silica as cobalt support for the Fischer–Tropsch Synthesis: Pretreatment, cobalt loading and particle size effects

The use of mesostructured materials as cobalt support for the Fischer–Tropsch Synthesis has taken increasing importance in the last decade. However, little use has been made of the hexagonal mesoporous silica, as most of the works have been reported for Co/MCM-41 and Co/SBA-15 catalytic systems. The effect of cobalt loading, impregnation method, particle size and pretreatment on the catalytic properties of Co/HMS catalysts for the Fischer–Tropsch Synthesis reaction have been studied.

The use of HMS as cobalt catalysts support for the Fischer–Tropsch Synthesis seems to be very promising. When  $\text{SiO}_2$  is used as support, the product distribution among the  $\text{C}_5^+$  hydrocarbons shows a marked tendency towards  $\text{C}_{19}^+$  fraction, while when HMS is used as support, the diesel fraction is favored. This result leads to the conclusion that the HMS pore structure produced a chain growth hindrance tailoring the product distribution towards the diesel fraction.

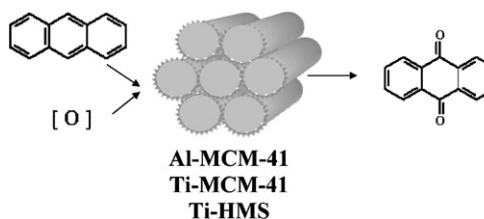


**R.S. Araújo, D.C.S. Azevedo, E. Rodríguez-Castellón, A. Jiménez-López, C.L. Cavalcante Jr.**

*Journal of Molecular Catalysis A: Chemical* 281 (2008) 154

Al and Ti-containing mesoporous molecular sieves: Synthesis, characterization and redox activity in the anthracene oxidation

Mesoporous materials H-MCM-41, Al-MCM-41(10), Ti-MCM-41(30) and Ti-HMS(30) were synthesized by the sol-gel method at room temperature. Samples have surface areas of 500–750  $\text{m}^2/\text{g}$ , high degree of isomorphic substitution and, in certain cases, significant acidity (Brønsted and Lewis). Studies of anthracene oxidation at 348 K showed that the Ti-HMS(30) sample is much more prone to redox catalysis (yield > 90%) than the other mesoporous samples. Such performance seems to be related to surface area, nature of the heteroatom introduced, Si/Ti molar ratio and strength and concentration of acid sites.

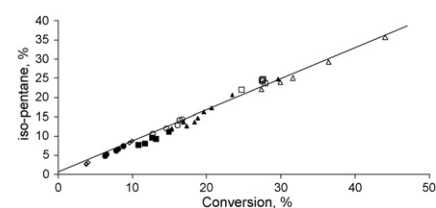


**L.N. Belandría, C.S. González, F. Aguirre, E. Sosa, A. Uzcátegui, G. González, J. Brito, S.L. González-Cortés, F.E. Imbert**

*Journal of Molecular Catalysis A: Chemical* 281 (2008) 164

Synthesis, characterization of FAU/EMT intergrowths and its catalytic performance in *n*-pentane hydroisomerization reaction

At 350 °C and with a carrier gas flow composition of  $\text{H}_2:\text{N}_2 = 2:1$ , the *iso*-pentane yield appeared to be a direct function of conversion, as shown in figure, for whatever structure (i.e. FAU, EMT or FAU/EMT) and at different times on stream. The slope of this curve is the selectivity; therefore, it appears to be independent of structure, time on stream, acidity, Pt/ $\text{H}^+$  ratio and metal dispersion, for this series of catalysts under these conditions (given temperature and carrier gas composition). From the slope is obtained a value of 82% selectivity.

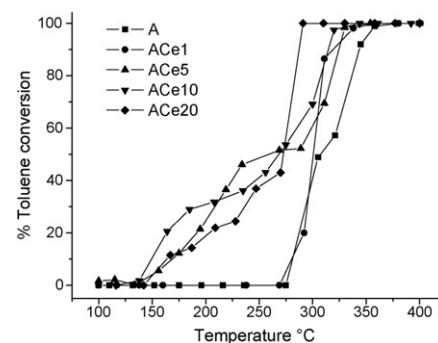


**G. Del Angel, J.M. Padilla, I. Cuauhtémoc, J. Navarrete**

*Journal of Molecular Catalysis A: Chemical* 281 (2008) 173

Toluene combustion on  $\gamma\text{-Al}_2\text{O}_3\text{-CeO}_2$  catalysts prepared from boehmite and cerium nitrate

The catalytic activity of  $\text{Al}_2\text{O}_3\text{-Ce}$  catalysts toward the total oxidation of toluene was plotted a “S-Shape” light-off curve. The effect of Ce content (1, 5, 10 and 20 wt% Ce) in the toluene combustion is evident since the displacement to lower temperature for the total combustion of toluene is of 89 °C for the Ce (20%) support in comparing with the alumina reference catalyst.

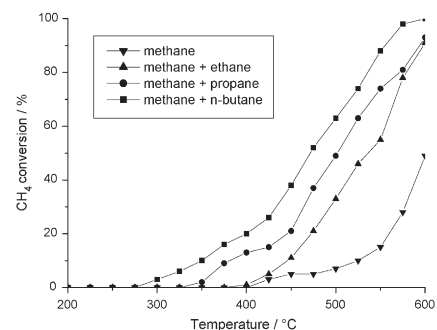


**Griselda Corro, Carlos Cano, J.L.Garcia Fierro**

*Journal of Molecular Catalysis A: Chemical* 281 (2008) 179

Promotional effect of C<sub>2</sub>–C<sub>4</sub> hydrocarbon on CH<sub>4</sub> oxidation on sulfated Pt/ $\gamma$ -Al<sub>2</sub>O<sub>3</sub> catalysts

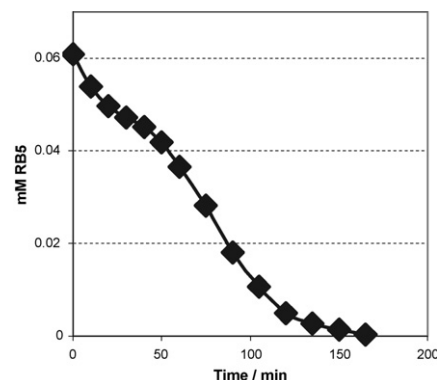
A very strong promotional effect of the presence of C<sub>2</sub>H<sub>6</sub>, C<sub>3</sub>H<sub>8</sub>, or n-C<sub>4</sub>H<sub>10</sub> in the reaction feed on complete oxidation of low concentrations of methane (2000 ppmV) under lean-burn conditions and in the presence of SO<sub>2</sub> was found over sulfated 1% Pt/ $\gamma$ -Al<sub>2</sub>O<sub>3</sub> catalyst. This promotional effect was further increased on 2% Pt/ $\gamma$ -Al<sub>2</sub>O<sub>3</sub>. Results are explained on basis of the probability of methane adsorption on the free Pt surface active sites. This probability increases (i) as the oxygen coverage over platinum surface is lowered by C<sub>2</sub>H<sub>6</sub>, C<sub>3</sub>H<sub>8</sub>, or n-C<sub>4</sub>H<sub>10</sub> oxidation and (ii) as the number of initial surface Pt sites increases.

**Yolanda Flores, Roberto Flores, Alberto Alvarez Gallegos**

*Journal of Molecular Catalysis A: Chemical* 281 (2008) 184

Heterogeneous catalysis in the Fenton-type system reactive black 5/H<sub>2</sub>O<sub>2</sub>

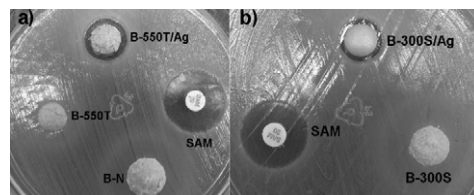
In this study, hydrogen peroxide is activated in the presence of a heterogeneous catalyst (Fe<sup>3+</sup>-containing ashes) to become a powerful oxidant that destroys reactive black 5, one of the most important azo dye in the dyeing industry. After 2 h of treatment, reactive solutions were effectively colorless and 80% of the original chemical oxygen demand was removed.

**S.M. Magaña, P. Quintana, D.H. Aguilar, J.A. Toledo, C. Ángeles-Chávez, M.A. Cortés, L. León, Y. Freile-Peigrín, T. López, R.M. Torres Sánchez**

*Journal of Molecular Catalysis A: Chemical* 281 (2008) 192

Antibacterial activity of montmorillonites modified with silver

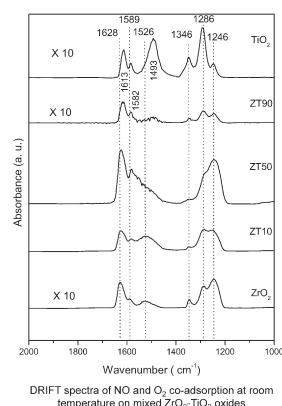
The antibacterial properties of Ag exchanged montmorillonites from Pellegrini Lake, Argentina were tested. Montmorillonite was submitted to: (a) calcination at 550 °C for 3 h and (b) grinding during 300 s; and then ion exchanged with silver. Growth inhibition of *E. coli* was measured by the antibacterial disk susceptibility test and the minimum inhibitory concentration (MIC) methods. Both montmorillonites showed good antibacterial activity after silver loading. The ground sample required a lower MIC to avoid *E. coli* growth than the thermally treated; although the last one showed a bigger inhibition zone in the disk susceptibility method. The results shows that the antibacterial activity is generated by the Ag<sup>+</sup> present in the clay, as confirmed by X-ray photoelectronic spectroscopy (XPS); however the overall antibacterial properties are affected by the availability of the ionic silver to be in contact with the bacteria.

**R. Pérez-Hernández, D. Mendoza-Anaya, M.E. Fernández, A. Gómez-Cortés**

*Journal of Molecular Catalysis A: Chemical* 281 (2008) 200

Synthesis of mixed ZrO<sub>2</sub>–TiO<sub>2</sub> oxides by sol–gel: Microstructural characterization and infrared spectroscopy studies of NO<sub>x</sub>

Single ZrO<sub>2</sub>, TiO<sub>2</sub> and mixed ZrO<sub>2</sub>–TiO<sub>2</sub> oxides with various Zr:Ti composition (90:10, 50:50 and 10:90) were prepared by sol-gel method. The samples were characterized by DSC, nitrogen adsorption, SEM, XRD, molecular simulation and DRIFT. An amorphous XRD pattern was observed in the ZT50 sample, this behavior was related to the Zr–O–Ti mixed bond formed which caused an atomic disorder in the structure of the sample and this result was confirmed by molecular simulation. Different kinds of surface nitrates (NO<sub>x</sub>, x = 2, 3) species were observed on the ZrO<sub>2</sub>–TiO<sub>2</sub> samples; these species are formed on Lewis sites and the amount of these species on the oxide surfaces runs parallel with the surface area, Zr/Ti ratio and mixed Zr–O–Ti bond population. On the Zr-rich samples the bridged and bidentate NO<sub>3</sub><sup>–</sup> species are the preferred coordination for these mixed oxides.

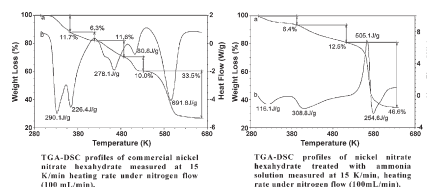


**Alfonso Loaiza-Gil, Marlin Villarroel, José F. Balbuena, María A. Lacruz, Sergio Gonzalez-Cortés**

*Journal of Molecular Catalysis A: Chemical* 281 (2008) 207

Thermal decomposition study of silica-supported nickel catalyst synthesized by the ammonia method

Comparison of TGA–DSC profiles of commercial nickel nitrate hexahydrate (left side) and nickel nitrate hexahydrate treated with ammonia solution (right side) lighted the effect of ammonia solution addition on commercial nickel salt. In fact, five steps of TGA decomposition pattern were observed on nickel nitrate hexahydrate and only three steps for the treated salt. Calculated molecular weight of treated nickel salt suggested that aqua ammine nickel ions were formed. DSC profiles of samples indicated a great structural rearrangement on the aqua ammine nickel ion before the last decomposition step. The first step of the chemistry involved in the silica-supported nickel catalyst preparation by the ammonia method was illustrated by comparison of such TGA–DSC profiles.

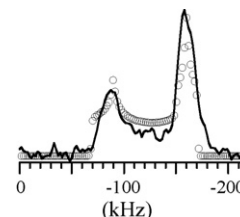


**Xuefeng Wang, Luis J. Smith**

*Journal of Molecular Catalysis A: Chemical* 281 (2008) 214

Solid-state NMR strategies for characterizing high surface area niobates

The niobium environment in  $KCa_2Nb_3O_{10}$  and its acid exchanged version were studied using  $^{93}Nb$  solid-state NMR. The change in the local environment of surface niobium sites upon acid exchange is observed via NMR derived electric field gradient information and attributed to changes in the terminal niobium–oxygen bonds.

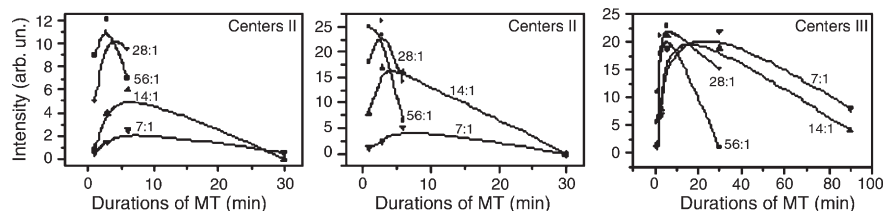


**M. Kakazey, M. Vlasova**

*Journal of Molecular Catalysis A: Chemical* 281 (2008) 219

About opportunities of the directed modification a set of defects in the surface region of ZnO particles

The quantitative analysis of the changes of intensity (concentration of the centers in the sample) of EPR-signals I–VI depending on conditions of mechanical treatment (MT) (speed of rotation of jars of a mill, duration of MT, amount of entered additives, etc.) has allowed to establish interrelation between defects formation and temperature processes, which develop during MT.

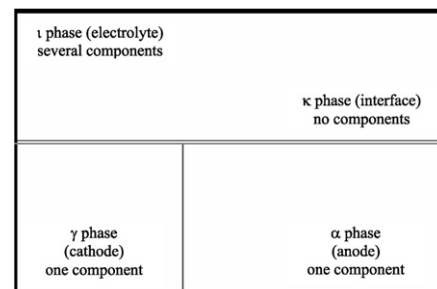


**F. León, A. Beakou, M.G. Amaya**

*Journal of Molecular Catalysis A: Chemical* 281 (2008) 226

Metal–electrolyte interface interaction on a negative electrochemical device

The negative electrochemical device is a heterogeneous surface system, consisting of multiple electrode galvanic micro-cells. The mass transfer due to irreversible redox reactions is assessed, in order to find the relationship between electrochemical and mechanical forces on the surface. A Gibbs ensemble is applied and a Young-Laplace equation is proposed for dealing with surface tension on the metal–electrolyte interface.



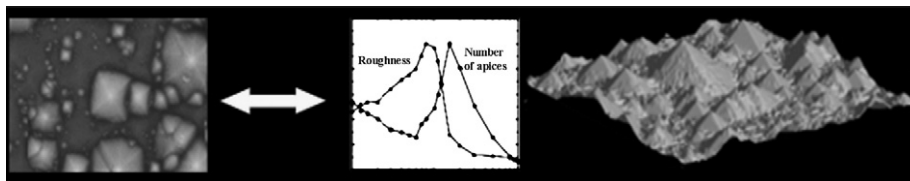


**M.P. Suárez, D.A. Mirabella, C.M. Aldao**

*Journal of Molecular Catalysis A: Chemical* 281 (2008) 230

Dynamics of hillocks formation during wet etching

Etch hillocks formation was studied experimentally and modeled using the Monte Carlo method. Simulations were used to explore the consequences of site-dependent detachment probabilities on surface morphology for a one- and two-dimensional substrate models. Comparison with pyramidal etch hillocks that are regularly observed in anisotropic etching of Si(1 0 0) are presented. The steady-state morphologies are analyzed and the hillock size distributions determined. The mechanisms responsible for the steady-state morphologies are described.



**N. Bajales Luna, F.J. Bonetto, R.A. Vidal, E.C. Goldberg, J. Ferrón**

*Journal of Molecular Catalysis A: Chemical* 281 (2008) 237

Low energy ion scattering in He/HOPG system

In this work, we study the neutralization of low energy  $\text{He}^+$  ions on graphite verifying that the ion fraction is close to null. Resonant neutralization to the ground state (RN) has been the main mechanism expected for  $\text{He}^+$  scattered by HOPG, but we found that only by including the resonant neutralization to the first excited state (1s, 2s), the small ion fractions measured can be explained.

